# Sequential generation of two distinct synapse-driven network patterns in developing neocortex.

Camille Allène, Adriano Cattani, James B. Ackman, Paolo Bonifazi, Laurent Aniksztejn, Yehezkel Ben-Ari, Rosa Cossart

Cellular/Molecular

# Sequential Generation of Two Distinct Synapse-Driven Network Patterns in Developing Neocortex

**Camille Allène, Adriano Cattani, James B. Ackman, Paolo Bonifazi, Laurent Aniksztejn, Yehezkel Ben-Ari, and Rosa Cossart**

Institut de Neurobiologie de la Méditerranée, Inserm U901, Université de la Méditerranée, 13273 Marseille cedex 9, France

**Developing cortical networks generate a variety of coherent activity patterns that participate in circuit refinement. Early network oscillations (ENOs) are the dominant network pattern in the rodent neocortex for a short period after birth. These large-scale calcium waves were shown to be largely driven by glutamatergic synapses albeit GABA is a major excitatory neurotransmitter in the cortex at such early stages, mediating synapse-driven giant depolarizing potentials (GDPs) in the hippocampus. Using functional multineuron calcium imaging together with single-cell and field potential recordings to clarify distinct network dynamics in rat cortical slices, we now report that the developing somatosensory cortex generates first ENOs then GDPs, both patterns coexisting for a restricted time period. These patterns markedly differ by their developmental profile, dynamics, and mechanisms: ENOs are generated before cortical GDPs (cGDPs) by the activation of glutamatergic synapses mostly through NMDARs; cENOs are low-frequency oscillations (~0.01 Hz) displaying slow kinetics and gradually involving the entire network. At the end of the first postnatal week, GABA-driven cortical GDPs can be reliably monitored; cGDPs are recurrent oscillations (~0.1 Hz) that repetitively synchronize localized neuronal assemblies. Contrary to cGDPs, cENOs were unexpectedly facilitated by short anoxic conditions suggesting a contribution of glutamate accumulation to their generation. In keeping with this, alterations of extracellular glutamate levels significantly affected cENOs, which are blocked by an enzymatic glutamate scavenger. Moreover, we show that a tonic glutamate current contributes to the neuronal membrane excitability when cENOs dominate network patterns. Therefore, cENOs and cGDPs are two separate aspects of neocortical network maturation that may be differentially engaged in physiological and pathological processes.**

*Key words:* **development; GABA; imaging; network; cortex; synchrony**

## Introduction

Spontaneous correlated neuronal activity is the hallmark of developing networks and plays a central role in their construction (Katz and Shatz, 1996; Khazipov et al., 2004; Cang et al., 2005; Kandler and Gillespie, 2005; Nicol et al., 2007). A variety of coordinated activity patterns have been described in developing neocortical structures from correlated pairs of neuronal precursor cells (Owens and Kriegstein, 1998) to gap junction-synchronized cortical columns (Yuste et al., 1992; Kandler and Katz, 1998; Dupont et al., 2006). Clarifying the underlying mechanisms and the spatiotemporal interactions between these diverse network patterns is crucial toward understanding their ultimate function in the construction of cortical maps.

Two synapse-driven network patterns have been extensively described in immature cortical structures: (1) Cortical early network oscillations (cENOs) are large-scale oscillatory calcium waves, occurring immediately after birth at low frequency and providing most of the coherent activity in the developing rodent neocortex (Garaschuk et al., 2000). Cortical ENOs require action potentials and are driven by NMDA and AMPA receptors but not $GABA_A$ receptors (Garaschuk et al., 2000; Corlew et al., 2004; McCabe et al., 2006). (2) Giant depolarizing potentials (GDPs) are the earliest synapse-driven network pattern in the developing hippocampus (Ben-Ari et al., 1989; Garaschuk et al., 1998; Crépel et al., 2007). They occur a few days after birth in rodents at moderate frequency (~0.1 Hz). They are driven by GABAergic transmission and disappear with the excitatory/inhibitory shift in the actions of GABA (Ben-Ari et al., 1989; Garaschuk et al., 1998; Tyzio et al., 2007).

Relying on the apparent similarities between these patterns, it was concluded that cENOs were the cortical counterpart to the hippocampal GDPs but generated by glutamatergic synapses, which would play a more critical role in the developing neocortex ("cortical GDPs") (McCabe et al., 2007). Therefore GDPs and cENOs would reflect intrinsic differences between brain structures. Yet, GABA also excites immature neocortical neurons (Yuste and Katz, 1991; Owens et al., 1996; Dammerman et al., 2000; Garaschuk et al., 2000; Marandi et al., 2002; Yamada et al., 2004; Tyzio et al., 2006; Ben-Ari et al., 2007) and the possibility that cENOs and GDPs could be separate network patterns se-

Received July 31, 2008; revised Sept. 30, 2008; accepted Oct. 5, 2008.

This work was supported by grants from Inserm, the Ville de Marseille and Région Provence-Alpes-Côte d'Azur, and the Agence Nationale Recherche (Programme Jeunes Chercheurs). R.C. is funded by the Centre National de la Recherche Scientifique. C.A. is funded by the Ministère de l'Education Nationale et de la Recherche. P.B. is funded by the Marie Curie Fellowship. We thank Sonja Martin for her contribution to the supplemental movies and Dr. Milh for helpful discussions.

Correspondence should be addressed to Dr. Rosa Cossart, Institut de Neurobiologie de la Méditerranée, Inserm U29, Parc Scientifique de Luminy, BP.13, 13273 Marseille cedex 9, France. E-mail: cossart@inmed.univ-mrs.fr.

DOI:10.1523/JNEUROSCI.3733-08.2008

 0270-6474/08/2812851-13$15.00/0

quentially dominating the developing neocortex has not been excluded.

To test this hypothesis we monitored the spatiotemporal patterns of neuronal activities in slices of rat somatosensory cortex between embryonic to postnatal stages using multibeam two-photon microscopy, on-line analysis, and targeted single-cell and field potential recordings. We show that the immature neocortex produces at birth cENOs and cortical synchronous plateau assemblies [cSPAs, i.e., synchronous calcium plateaus associated with intrinsic membrane potential oscillations in restricted groups of neurons, identical to the recently described activity in the hippocampus (Crépel et al., 2007)], then GABA-driven GDPs that are similar to hippocampal GDPs. These patterns differed in their spatiotemporal dynamics, intracellular correlates, developmental profile, and pharmacological features. Indeed, cENOs were generated by the activation of NMDARs and favored by higher extracellular glutamate levels in contrast to cGDPs which preferentially involved GABAergic transmission. Remarkably, a tonic glutamate current excited neurons at the stage when cENOs were preferentially observed. Finally, we show that cENOs and cGDPs present a differential sensitivity to anoxic conditions since the occurrence of cGDPs was impaired while cENOs were transiently increased, in anoxic/aglycemic or low rate saline perfusion. We conclude that the neocortex successively generates two coherent activity patterns, first cENOs then cGDPs. This developmental sequence results in differential sensitivity to ischemia during maturation.

**Table 1. Quantitative comparison between cENOs and cGDPs in cortical slices**

| | cENO | cGDP |
|---|---|---|
| Age | | |
| E20 | | |
| Incidence | 0/11 | 0/11 |
| P0–P4 | | |
| Amp | 38 ± 3 ($n = 53$) | |
| Freq (per min) | 2.45 ± 0.3 ($n = 53$) | |
| Incidence | 53/110 | 1/3 |
| P5–P9 | | |
| Amp | 41 ± 13 ($n = 3$)* | 13 ± 3 ($n = 63$) |
| Freq (per min) | 3.25 ± 2.26 ($n = 3$)* | 8.4 ± 0.7 ($n = 63$) |
| Incidence | 3/48 | 63/137 |
| Orientation of slices | | |
| Coronal | | |
| Amp | 47 ± 29 ($n = 2$)* | 7 ± 1 ($n = 12$) |
| Freq (per min) | n.a. | 6.81 ± 1.07 ($n = 12$) |
| Incidence | 2/42 | 12/27 |
| Horizontal | | |
| Amp | 39 ± 3 ($n = 56$)* | 16 ± 1 ($n = 64$) |
| Freq (per min) | 2.55 ± 0.34 ($n = 56$)* | 9.2 ± 0.8 ($n = 64$) |
| Incidence | 56/158 | 64/140 |
| Pharmacology | | |
| Bicuculline | | |
| Amp (% cont) | 111 ± 25 ($n = 9$)* | 9 ± 7 ($n = 9$) |
| Freq (% cont) | 153 ± 72 ($n = 9$)* | 0 ($n = 9$) |
| D-APV | | |
| Amp (% cont) | 13 ± 6 ($n = 13$)* | 54 ± 21 ($n = 5$) |
| Freq (% cont) | 22 ± 1 ($n = 13$)* | 70 ± 5 ($n = 5$) |
| D-APV + NBQX | | |
| Amp/cont (%) | 7 ± 7 ($n = 14$)* | 80 ± 17 ($n = 6$) |
| Freq/cont (%) | 5 ± 1 ($n = 14$)* | 14 ± 14 ($n = 6$) |
| Calcium events kinetics | | |
| Rise time (s) | 1.02 ± 0.02 ($n = 1000$)* | 0.230 ± 0.005 ($n = 1000$) |
| Decay (s) | 5.32 ± 0.2 ($n = 1000$)* | 1.02 ± 0.2 ($n = 1000$) |
| Synchronicity duration (s) | 0.97 ± 0.11 ($n = 1000$)* | 0.25 ± 0.05 ($n = 1000$) |
| Patch-clamp recordings | | |
| Amplitude (mV) | 12.8 ± 2.5 ($n = 9$) | 12.4 ± 4.4 ($n = 4$) |
| Duration (s) | 2.4 ± 0.8 ($n = 9$)* | 0.28 ± 0.0 ($n = 4$) |
| Rise time (s) | 0.6 ± 0.2 ($n = 9$)* | 0.05 ± 0.0 ($n = 4$) |
| AP number | 3.5 ± 1.5 ($n = 9$) | 4.2 ± 0.0 ($n = 4$) |
| Firing frequency (Hz) | 1.9 ± 0.5 ($n = 9$)* | 15.4 ± 0.5 ($n = 4$) |
| Frequency (per min) | 1.6 ± 0.5 ($n = 9$)* | 8.2 ± 0.8 ($n = 4$) |
| Field potential recordings | | |
| Amplitude ($\mu$V) | 142 ± 58 ($n = 5$) | 43 ± 9 ($n = 7$) |
| Duration (s) | 2.7 ± 0.3 ($n = 5$)* | 0.5 ± 0.4 ($n = 7$) |
| Peak frequency (Hz) | 15.3 ± 3.9 ($n = 5$) | n.a. |
| Rate of occurrence (Hz) | 0.010 ± 0.007 ($n = 5$)* | 0.15 ± 0.03 ($n = 7$) |
| MUA (Hz) | 28.6 ± 7.8 ($n = 5$) | 14.6 ± 2.5 ($n = 7$) |

Amp, Amplitude; AP, action potential; Freq, frequency; n.a., not applicable. See Materials and Methods. Bicuculline, 10 $\mu$M, D-APV, 40 $\mu$M; NBQX, 10 $\mu$M.
*$p < 0.05$ compared with cGDPs.

## Materials and Methods

*Slice preparation and calcium imaging.* Coronal and horizontal slices of somatosensory cortex (400–450 $\mu$m thick) were prepared from E20 to 9-d-old (P9) Wistar rats using a Microm tissue slicer (International) in ice-cold oxygenated modified artificial CSF (mACSF: 0.5 mM $CaCl_2$ and 7 mM $MgSO_4$; NaCl replaced by an equimolar concentration of choline). Most of the experiments were performed on horizontal slices since the incidence of calcium waves (cENOs) was critically diminished in coronal slices (see Table 1) (Garaschuk et al., 2000; Corlew et al., 2004; Sun and Luhmann, 2007). Slices were then transferred for rest (~1 h) in oxygenated normal ACSF containing (in mM): 126 NaCl, 3.5 KCl, 1.2 $NaH_2PO_4$, 26 $NaHCO_3$, 1.3 $MgCl_2$, 2.0 $CaCl_2$, and 10 D-glucose, pH 7.4. For AM-loading, slices were incubated in a small vial containing 2.5 ml of oxygenated ACSF with 25 $\mu$l of a 1 mM fura-2 AM solution (Molecular Probes; in 100% DMSO) for 20–30 min. Slices were incubated in the dark, and the incubation solution was maintained at 35°–37°C. The fraction of labeled cells was constant for all age groups included in the study (at P1: 6 ± 3% cells were visible in transmitted light but not in the calcium fluorescence image, $n = 1391$ cells, vs 5 ± 1% at P8, $n = 888$ cells, $p = 0.9$). Unless indicated otherwise, slices were perfused at a rate of 4 ml/min with continuously aerated (95% $O_2$/5% $CO_2$) normal ACSF at 35–37°C. Imaging was performed with a multibeam two-photon laser scanning system (Trimscope-LaVision Biotec) coupled to an Olympus microscope as previously described (Crépel et al., 2007). Images were acquired through a CCD camera (La Vision Imager 3QE), which typically resulted in a time resolution of ~100 ms (2 × 2 binning, pixel size: 600 nm). Slices were imaged using a low-magnification, high-numerical-aperture objective (20×, NA 0.95, Olympus). The size of the imaged field was typically 430 × 380 $\mu m^2$. Imaging depth was on average 80 $\mu$m below the surface (range: 50–100 $\mu$m).

*Analysis.* As previously described (Crépel et al., 2007), analysis of the calcium activity was performed with custom-made software written in Matlab (MathWorks). This program aimed at the automatic identification of loaded cells and at measuring their fluorescence as a function of time. The calcium signal of each cell was the average fluorescence within the contour of that cell, measured as a function of time.

The entire procedure could be performed on-line sufficiently quickly

to identify cells for targeted patch-clamp recordings. Signal-processing algorithms of MiniAnalysis software (Synaptosoft) were used to detect the onsets and offsets (time of half-amplitude decay) of calcium signals within the traces of individual cells. Active cells are neurons exhibiting at least one calcium event within the period of recording. Kinetics analysis of individual calcium events was performed using the MiniAnalysis program. Single and averaged events were fully characterized: rise times (10–90%), amplitudes, and decay time constants were calculated (single exponential fit). For SPA-associated events we chose to calculate the duration of individual calcium plateaus (time between the event onset and the start of the decay) instead of rise and decay times because the values of both parameters were negligible compared with the duration of the plateau. To compute the activity correlation of two cells, the onset of each event was represented by a Gaussian ($s = 1$ frame, to allow some jitter). The inner product of the resulting values was then calculated. The significance of each correlation value was estimated by direct comparison with a distribution computed from surrogate data sets, in which the events were randomly reshuffled in time. To quantify synchronous activity patterns (i.e., cENOs and cGDPs), we used four parameters: frequency, incidence, amplitude, and duration of synchronicity. The frequency of a network pattern was the averaged time interval between two peaks of synchronous activity. The incidence was the fraction of slices in which it could be recorded at least once. The amplitude of a network pattern in a given movie was the average of the maximum of cells coactive in each peak of synchrony across the movie. To identify peaks of synchronous activity that included more cells than expected by chance, we used interval reshuffling (randomly reordering of intervals between events for each cell) to create a set of surrogate event sequences. Reshuffling was performed 1000 times for each movie, and a surrogate histogram was constructed for each reshuffling. The threshold corresponding to a significance level of $p < 0.05$ was estimated as the number of coactive cells exceeded in a single frame in only 5% of these histograms. This threshold was used to calculate the duration of a synchronous activity pattern that is the number of successive frames for which the number of coactive cells was superior to threshold. Experimental values are given as means ± SEMs. Student's *t* test and $\chi^2$ test were used for statistical comparisons. $p < 0.05$ was considered significant.

*Electrophysiology.* Neurons were recorded using the patch-clamp technique in the whole-cell configuration. For voltage-clamp the composition of the intracellular solution was: 120 mM Cs-gluconate, 10 mM $MgCl_2$, 0.1 mM $CaCl_2$, 1 mM EGTA, 5 mM $Na_2$ adenosine triphosphate, 10 mM HEPES. With this solution glutamate-R-mediated postsynaptic currents (PSCs) reversed at +10 mV while $GABA_A$R-mediated PSCs reversed at −60 mV. Liquid junction potential value was −16.8 mV, but no correction was applied. For current clamp, the intracellular solution was: 130 mM K-methyl$SO_4$, 5 mM KCl, 5 mM NaCl, 10 mM HEPES, 2.5 mM Mg-ATP, and 0.3 mM GTP. No correction for liquid junction potential was applied.

The osmolarity was 265–275 mOsm, pH 7.3. Microelectrode resistance was 4–8 MΩ. Uncompensated access resistance was monitored throughout the recordings. Values <20 MΩ were considered acceptable and the results were discarded if it changed by >20%. Whole-cell measurements were filtered at 3 kHz using a patch-clamp amplifier (HEKA, EPC10). Recordings were digitized on-line (20 kHz) with a Labmaster interface card to a personal computer and acquired using Axoscope 7.0 software (Molecular Devices). Synchronization between optical and electrical signals was achieved by feeding simultaneously the Labmaster interface card with the trigger signals for each movie frame and the electrophysiological recordings. Neurons were also patch clamped without dye loading. In these conditions, we found electrophysiological events corresponding to GDPs or ENOs similar to which we found in dye loading conditions. Recordings were analyzed using the MiniAnalysis software (Synaptosoft). Extracellular recordings were performed with a glass pipette (~1 MΩ) filled with ACSF and the signal was recorded with a DAM80 amplifier (WPI). Spectrograms were calculated using the function "spectrogram" of Matlab (MathWorks).

*Pharmacology.* Antagonists for $GABA_A$ and ionotropic glutamate receptors mentioned in this manuscript are bicuculline (10 μM), gabazine (10 μM), NBQX (10 μM), and D-APV (40 μM). All drugs except TTX (Tocris) were purchased from Sigma. As previously described (Min et al., 1998), GPT (porcine heart, 115 kDa dimer) was dialyzed for 3 h with a 10 kDa cutoff membrane (Slide-A-Lyzer, Pierce Chemical) before the experiments. We confirmed that GPT was acting by scavenging glutamate by comparing the current evoked by pressure application of glutamate (1 mM) onto the same neuron recorded in voltage clamp at +40 mV in the absence or in the presence of GPT 5 U/ml (together with pyruvate 2 mM) in the puff pipette. As expected, currents evoked in the presence of the glutamate scavenger were significantly smaller ($n = 12$, $p < 0.05$, data not shown). Finally, we also confirmed that GPT did not affect network activity in the absence of pyruvate (frequency and amplitude of cENOs under GPT 5 U/ml (without pyruvate) were not significantly different relative to control: 140 ± 4%, $p = 0.4$ and 87 ± 2%, $p = 0.6$, respectively, $n = 3$).

## Results

### Maturation of population coherence in neocortical slices

We used multibeam two-photon imaging in horizontal slices including the primary somatosensory cortex, loaded with a calcium indicator (fura-2 AM), to record movies of spontaneous activity in rats aged between E20 and P9. We focused on the somatosensory area (39,166 cells, 238 cells per movie on average; 4000 frames/movie, 100 ms/frame). Analysis was performed using custom software to measure fluorescence changes in each cell and mark the onset and offset of individual calcium transients (Fig. 1) (see also Crépel et al., 2007). Four maturation steps of spontaneous neuronal activity could be distinguished:

At embryonic stages (E20), only a minority of cells were active (9 ± 0.02%, $n = 11$ slices, 3190 cells). Most activity consisted of sporadic calcium spikes (6.3 ± 1.6 s duration, $n = 433$ events, Fig. 1) that were poorly correlated between neurons (0.07% cell pairs significantly correlated, see Materials and Methods). Current-clamp recordings from active neurons revealed that these calcium events corresponded to immature action potentials (Fig. 1).

Around birth (P0–P3), more cells generated calcium spikes but another pattern appeared in approximately one third of active cells (32 ± 3% at P0, $n = 41$ slices) consisting of synchronous calcium plateaus (duration: 18.5 ± 2.3 s, 0.02 ± 0.001 Hz, $n = 493$ events, significantly different from calcium spikes in terms of duration, $p = 0.009$; 14% cell pairs significantly correlated) (Fig. 1). These were reminiscent of synchronous plateau assemblies (SPAs), recently described in the hippocampus (Fig. 1) (Crépel et al., 2007). Targeted current-clamp recordings showed that these plateaus corresponded to recurrent burst discharges when cells were recorded at $V_{rest}$ ($n = 5$ cells) (Fig. 1). Like hippocampal SPAs, cortical SPAs (cSPAs) were not synapse driven since they were not affected by blocking AMPA/KARs, NMDARs, and $GABA_A$Rs (fraction of SPA-cells in NBQX 10 μM, D-APV 40 μM, and bicuculline 10 μM, was 133 ± 14% of control, $n = 25$ slices, $p = 0.15$, data not shown). They were in contrast blocked by sodium and L-type calcium channel antagonists (to 15 ± 6% of control in the presence of TTX 1 μM and nifedipine 10 μM, $n = 3$ slices, $p = 0.003$, data not shown). Finally, as in the hippocampus, the emergence of cSPAs was controlled by signaling molecules involved during delivery since treatment with oxytocin (1 μM) of slices from rat fetuses (E20) having been initially intracardially perfused with ACSF to wash out the endogenous hormone, caused an almost two-fold increase in the fraction of SPA-cells to levels comparable to birth stages (37 ± 6% of SPA-cells at E20 in the presence of OT, vs 18 ± 2% of SPA-cells in control at E20, $n = 25$ movies, 5369 cells, $p = 0.03$, data not shown). In contrast, the fraction of active cells relative to the total number of imaged neurons was not affected by the hormone (active cells: 9 ± 2% at E20 control vs 8 ± 2% at E20 in OT, $p = 0.67$).

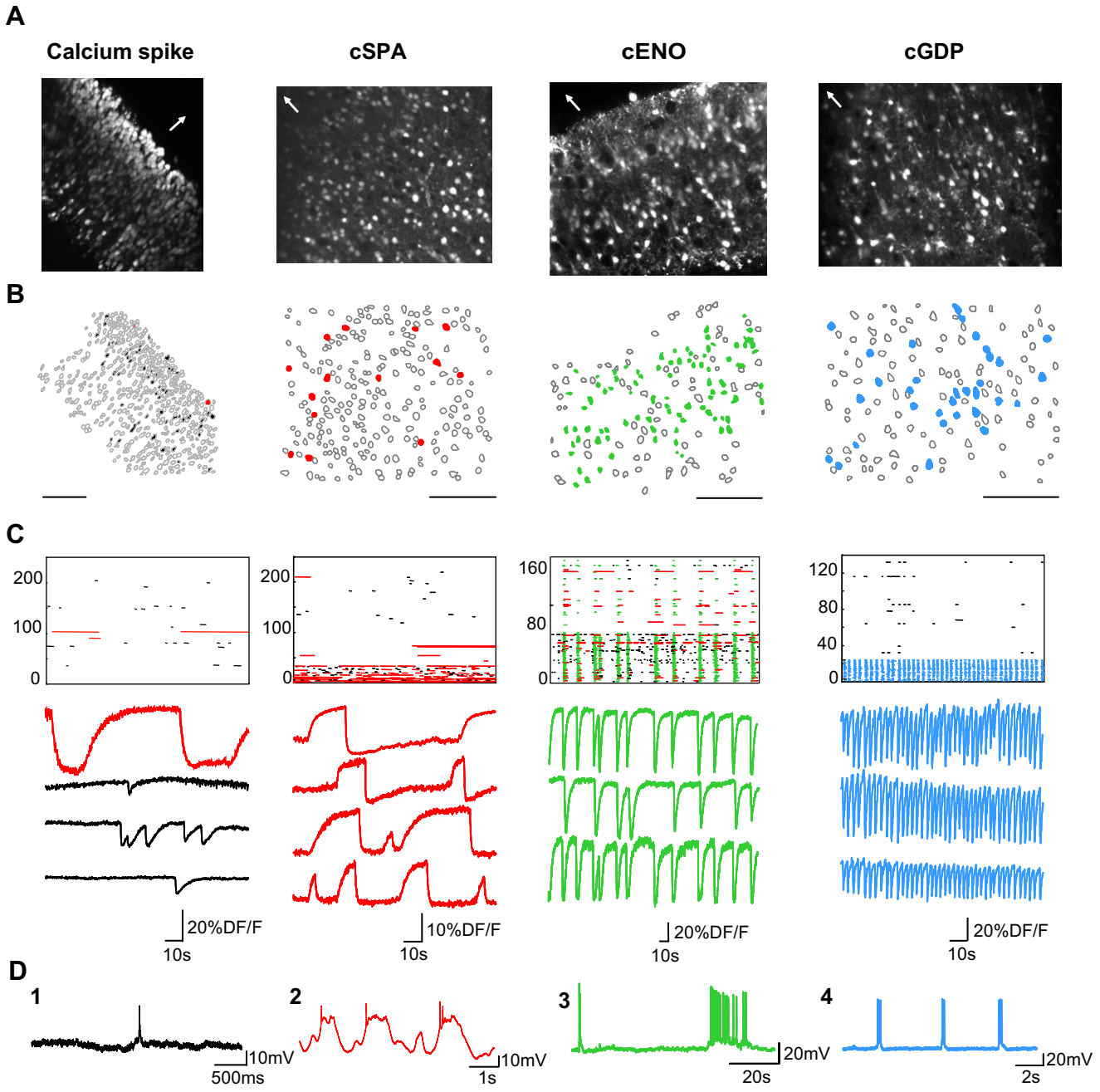


**Figure 1.** Multibeam two-photon imaging of the four maturation steps of spontaneous neuronal activity in somatosensory cortical slices from embryonic stages to first postnatal days. ***A***, Two-photon calcium fluorescence images of rat somatosensory cortical slices of the four types of spontaneous activity: calcium spikes (left), cortical synchronous plateau assemblies (cSPAs), cortical early network oscillations (cENOs), and cortical giant depolarizing potentials (cGDPs, right) recorded at E20, P0 (cortical plate), P3 (cortical plate, horizontal slice), and P7 (deeper layers), respectively. White arrows indicate direction of pial surface. ***B***, Automatically detected contours of the cells from the fluorescence images: open contours indicate silent cells, black filled contours indicate cells producing calcium spikes, red filled contours are cSPAs-cells, green filled contours are cENO cells, and blue filled contours are cGDPs-cells; scale bar: 100 $\mu$m. ***C***, Raster plots of the activity from the four slices illustrated in ***A*** in control ACSF. Each row represents a single cell and each horizontal line the duration of detected calcium transients. Four populations of events can be distinguished as shown by representative fluorescence traces below the raster plots (black: calcium spikes; red: calcium plateaus i.e., cSPA-events; green: cENO-events; blue: cGDP-events). ***D***, Current-clamp recordings ($V_{rest}$ of approximately $-60$ mV) in four representative neurons displaying the four types of calcium activities described above. ***D1***, A calcium spike recorded in a neuron at E20. ***D2***, Red: cSPA recorded in a neuron at P0. Note that calcium plateaus are associated to rhythmic membrane potential oscillations as SPAs described in the hippocampus. ***D3***, Green: a cortical ENO. ***D4***, Blue: three successive cortical GDPs.

During the same developmental period as cSPAs were observed (P0–P3), we could image, in almost half of the slices, synchronous waves of calcium activity slowly invading the entire network and sharing spatiotemporal dynamics comparable to those previously described for cENOs (Figs. 1, 2, Table 1; supplemental Movie 2, available at www.jneurosci.org as supplemental material) (Garaschuk et al., 2000; Corlew et al., 2004; Sun and Luhmann, 2007). Indeed, they were associated with calcium events having slow kinetics (Fig. 3, Table 1) occurred at the same rate (1.5 ± 0.3 waves/min on average) during the same developmental period (P0–P5) (see Fig. 3), and could be detected in almost all neurons within a given cortical region (average fraction of active cells involved in cENOs was 81 ± 3%). Even neurons involved in cSPAs tended to synchronize within ENOs (on aver-

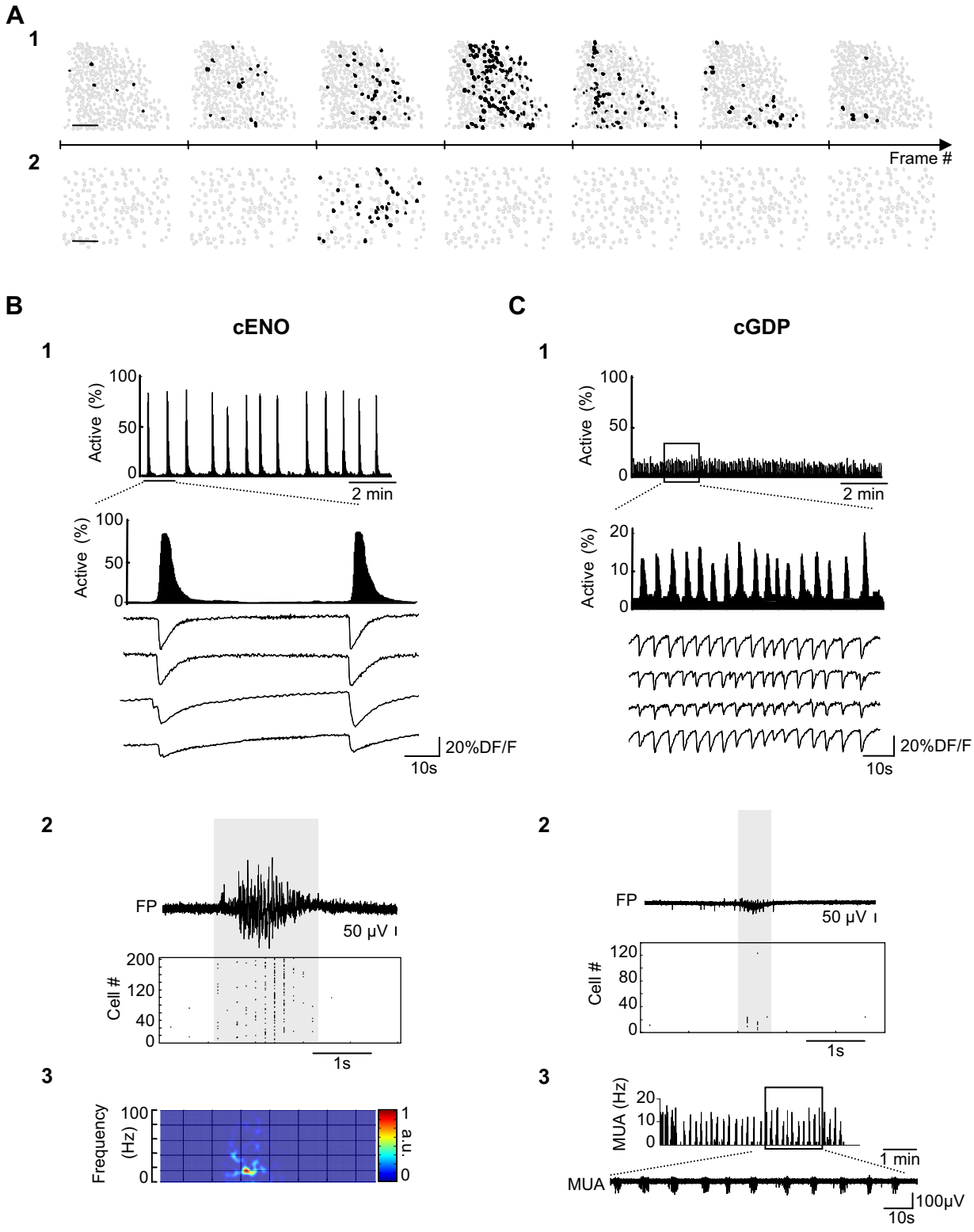


**Figure 2.** Cortical ENOs and GDPs display two distinct spatiotemporal dynamics. ***A1***, ***A2***, Contour maps of seven successive movie frames taken from a P3 (***A1***) and a P8 (***A2***) horizontal somatosensory slice to illustrate the slower dynamics of cENOs (***A1***) compared with cGDPs (***A2***). Black filled contours indicate cells active in frames where network synchronization reaches significance threshold (see Materials and Methods). One frame every 150 ms; scale bar: 100 $\mu$m ***B1***, Histogram indicating the fraction of imaged cells detected as being active for each movie frame in a P1 horizontal somatosensory cortical slice. Each peak of the histogram represents a cENO. Calcium fluorescence traces of four cells implicated in the two cENOs illustrated in the above histogram on an expanded time scale. ***B2***, Simultaneous field potential recording (FP) and calcium imaging (raster plot) during a cENO occurring in a P3 horizontal cortical slice. Raster plot indicates the onset of each calcium event in all imaged cells as a function of time. Note the strong correlation between field potential oscillations and multineuron calcium activity. ***B3***, Spectrogram of the FP oscillation associated to the cENO illustrated in ***B2***. a.u.: arbitrary units. ***C1***, ***C2***, Same as ***A1*** and ***A2*** but in a P6 somatosensory horizontal slice where cGDPs could be recorded (small peaks of synchrony). Note that peaks associated with cGDPs are much smaller and more frequent than those associated with cENOs (***B2***). They involve fewer cells as shown in the ***C2*** raster plot. ***C3***, Cortical GDPs are not associated with any remarkable oscillatory pattern but correspond to a significant increase in MUA as shown by the frequency histogram of MUA as a function of time and by the MUA recording trace below.

age 71 ± 4% of SPA-cells were involved in cENOs in the form of synchronous calcium plateaus, $n = 6$). Interestingly, in contrast to other patterns described here, the incidence of these waves was significantly affected by the slice orientation (see Table 1 and Materials and Methods). These calcium waves were tightly correlated to changes in the field potential and increased multiunit activity (see Table 1, Fig. 2). Targeted current-clamp recordings performed while imaging indicated that these waves were associated with slowly rising and prolonged membrane potential depolarizations (Fig. 3, Table 1) whereas voltage clamp recordings indicated that they were associated with increased synaptic activity ($n = 11$) (see Fig. 5*A3*). Most importantly, these calcium oscillations presented the same pharmacological profile as cENOs since their occurrence was not affected by $GABA_AR$ blockade ( $p = 0.66$) (Table 1, Fig. 4), but completely prevented by AMPA/KAR and NMDAR antagonists (Table 1) ( $p = 0.08$). Therefore the large calcium waves and field potential oscillations we recorded, corresponded to the previously described cENOs (Garaschuk et al., 2000). We have now provided the intracellular correlates for these network oscillations in voltage- and current-clamp recordings.

Last, starting from P6, a coherent pattern reminiscent of the GDPs initially described in the hippocampus (Ben-Ari et al., 1989), was recorded in almost half of the slices (46%, $n = 137$ slices, see also Table 1; supplemental Movie 1, available at www.jneurosci.org as supplemental material) while the occurrence of cSPAs significantly declined (SPA-cells: 16 ± 3% of active cells in slices where cGDPs could be recorded, $n = 24$ movies, $p = 0.0002$) (Fig. 3). Pharmacological and electrophysiological observations indicated that this pattern indeed corresponded to GDPs. Cortical GDPs consisted of recurrent synchronous calcium oscillations occurring on average at 0.1 Hz (0.14 ± 0.01 Hz, see Table 1) and involving a subpopulation of neurons (13 ± 3% neurons involved on average, $n = 24$ slices). They were often confined within deeper cortical layers (Fig. 1) and always associated to fast calcium events (see Table 1, Fig. 3) occurring simultaneously within one movie frame (i.e., <100 ms) (Fig. 2). Extracellular recordings further confirmed that these synchronous fast calcium events were associated to field potential changes and to a marked increase in multiunit activity (Fig. 2, Table 1). These oscillations were strongly dependent on the actions of GABA as they were almost completely blocked by the $GABA_AR$ antagonist (bicuculline 10 $\mu$M, $n = 9$ slices) (Fig. 4, see Table 1). As in the hippocampus, cGDPs also required glutamatergic transmission since their frequency was significantly reduced by blockade of AMPA/KARs and NMDARs (to 14 ± 14% of control values in NBQX 10 $\mu$M, D-APV 40 $\mu$M, $n = 6$ slices, $p = 0.004$) (Fig. 5). However, the fraction of cells involved in cGDPs was not significantly affected by AMPA/KAR and NMDAR blockers (to 80 ± 17% of control, $n = 6$, $p = 0.2$). Last, current-clamp recordings confirmed that these calcium oscillations corresponded to recurrent suprathreshold membrane potential depolarizations (Table 1, Figs. 1, 3) whereas voltage-clamp recordings validated that they were associated with bursts of synaptic postsynaptic events (sPSCs, $n = 4$) (Fig. 5*B3* and Materials and Methods).

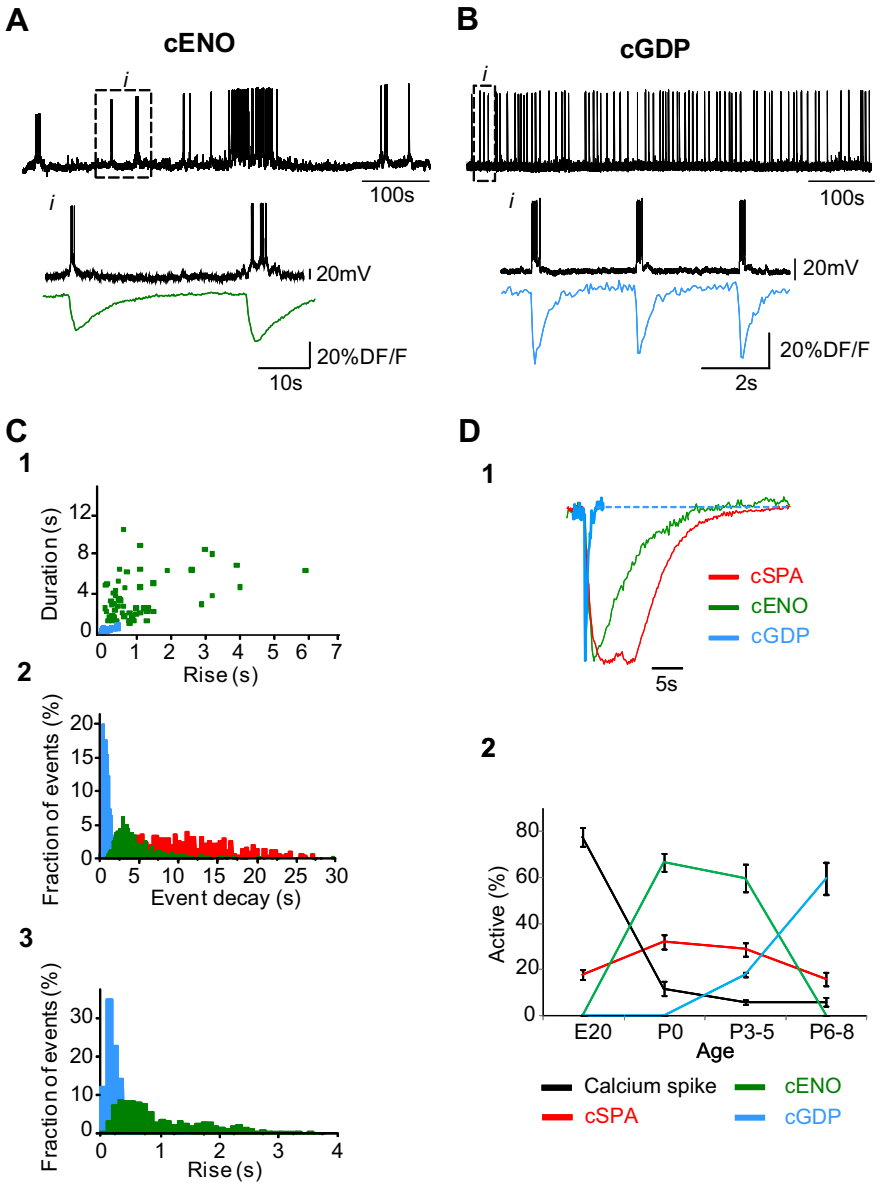


**Figure 3.** Single-cell electrophysiological and calcium events associated with cortical ENOs and GDPs. ***A***, ***B***, Current-clamp recordings at resting membrane potential and corresponding calcium fluorescence traces (bottom traces) of cells implicated in cENOs (***A***) and cGDPs (***B***). Recording periods indicated in i are illustrated on an expanded time scale. ***C1***, Plots of the duration versus rise time of individual membrane potential oscillations associated with cGDPs (blue squares, $n = 4$ cells, 75 events) and cENOs (green, $n = 5$ cells, 65 events). ***C2***, ***C3***, Normalized distribution of the decay (2) and rise (3) times of single calcium events associated with cGDPs (blue, $n = 1000$) and cENOs (green, $n = 1000$). Distribution of the duration of the calcium plateaus associated with cSPAs (red, $n = 500$, see Materials and Methods) is also plotted in ***C2***. ***D1***, Comparison of three representative normalized calcium fluorescence traces recorded in single cells during cGDPs, cENOs, and cSPAs clearly illustrates the kinetics difference between these events. ***D2***, Graph indicates the fraction of calcium spike-, cSPA-, cENO-, and cGDP-cells relative to the number of active cells at four successive age groups between embryonic to first postnatal stages. Error bars indicate SEMs.

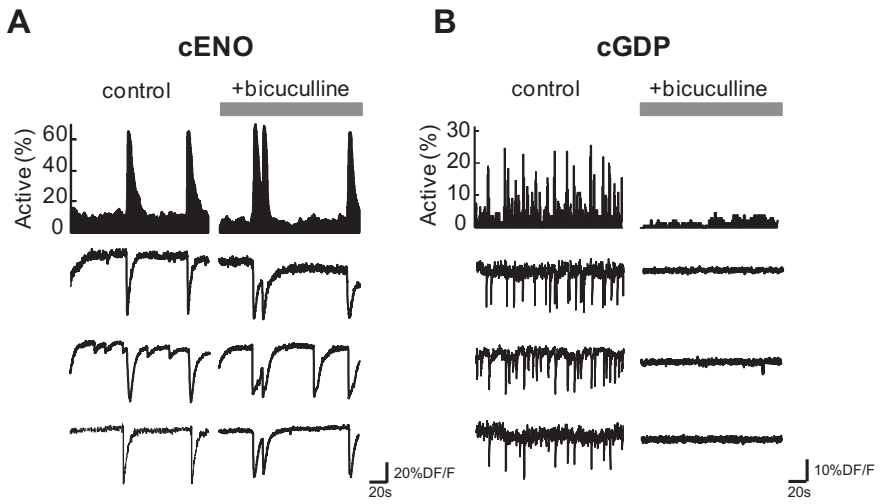


**Figure 4.** GABAergic transmission is not involved in the generation of cENOs but is crucial for cGDPs. ***A***, ***B***, Representative histograms indicating the fraction of imaged cells detected as being active for each movie frame as a function of time in a P3 (***A***) and a P8 (***B***) somatosensory horizontal slice. The occurrence of cENOs (peaks of synchrony in ***A***) was not significantly affected in the presence of the $GABA_AR$ antagonist (bicuculline, 10 $\mu$M) compared with control conditions. In contrast, cGDPs (peaks of synchrony in ***B***) were blocked in the presence of bicuculline. Below, Calcium fluorescence traces of three representative cells implicated in cENOs (***A***) and cGDPs (***B***) in control and after adding bicuculline.

Therefore, we found a sequence for the maturation of population coherence in the neocortex almost similar to the one previously described in the hippocampus (Crépel et al., 2007) except from the fact that two synapse-driven network patterns (cENOs and cGDPs), sequentially led the developing neocortex.

### Cortical ENOs differ from cortical GDPs

Figures 2–7 illustrate the major differences between cENOs and cGDPs recorded at the time when they dominate the activity of the immature cortical network (P0–P3 for cENOs and P6–P8 for cGDPs) (see Fig. 3*D2*). A comparative quantitative description of these two coherent patterns is provided in Table 1. Most electrophysiological and optical measurements used to assess network activity, including kinetics of individual calcium events, spatiotemporal dynamics, rates of occurrence or duration, significantly differed between cENOs and cGDPs ($p < 0.05$). Moreover, whereas both types of activity required synaptic transmission (as assessed with voltage clamp recordings), cENOs were glutamate driven, whereas GABA plays a critical role in the generation of cGDPs (see above). We next performed a series of experiments aimed at further discriminating between the mechanisms of generation of cENOs and cGDPs. First, we observed that NMDAR blockade alone significantly affected the occurrence of cENOs (to 21 ± 15% of control in D-APV 40 $\mu$M, $n = 11$, $p = 0.002$) (Table 1, Fig. 5), compared with cGDPs (to 70 ± 5% of control in D-APV 40 $\mu$M, $n = 5$, $p > 0.05$) (Table 1, Fig. 5) further confirming the crucial role of NMDAR activity in the generation of synchronous network oscillations in the immature neocortex (Garaschuk et al., 2000; Demarque et al., 2004; Dupont et al., 2006). The major contribution of NMDARs activation to the synaptic influx associated with cENOs was further established by measurements of their current–voltage relationship. Indeed, *I*/*V* curves associated with cENOs displayed a region of negative slope at hyperpolarized membrane potentials and reversed polarity close to 0 mV (2.5 ± 1.4 mV, $n = 4$ cells) (Fig. 5) whereas *I*/*V* curves corresponding to cGDPs were linear and reversed at more negative values (−40.5 ± 0.5 mV, $n = 4$ cells) (Fig. 5) clearly indicating an important $GABA_AR$ contribution. Interestingly, in addition to mediating cENOs-associated PSCs, we observed, in a majority of tested neurons (57%, $n = 14$, P1–P3), that NMDARs also provided a constant membrane potential depolarization most likely sustained by a tonic NMDAR current, since addition of D-APV induced a reversible hyperpolarization at resting membrane potential in current-clamp recordings (−6.3 ± 2.3 mV, $n = 4$) (supplemental Fig. 1, available at www.jneurosci.org as supplemental material) and an outward current at +40 mV in voltage-clamp mode (22 ± 6 pA, $n = 4$) (supplemental Fig. 1, available at www.jneurosci.org as supplemental material). Part of these effects was specific for younger rats (P1–P3). Indeed, NMDAR blockade did not affect resting membrane potential at developmental stages when cENOs are no longer observed (P8–P9, $n = 6$) (supplemental Fig. 1, available at www.jneurosci.org as supplemental material), whereas D-APV application still produced an outward current at +40 mV in voltage-clamp mode (15 ± 3 pA, $n = 3$).

As the above experiments suggested a contribution of NMDAR-driven tonic depolarization to the generation of cENOs, we decided to test whether such depolarization could be mimicked by elevating extracellular potassium concentrations in the presence of D-APV. Indeed, similar experiments were conducted in a previous study to argue that a tonic depolarizing drive provided by excitatory GABAergic transmission was instructive for the generation of hippocampal GDPs (Sipilä et al., 2005). We observed that if synchrony could be restored by 8 mM extracellular potassium, it was difficult to compare such network events to control cENOs since their amplitude was significantly decreased (to 43 ± 8% of control, $n = 8$, $p = 0.013$) while their frequency tended to increase (335 ± 171%, $n = 5$, $p = 0.135$) (supplemental Fig. 2, available at www.jneurosci.org as supplemental material). Likewise, in slices where cGDPs occurred (P8–P9), we observed that peaks of synchronous activity could indeed be restored in the presence of the $GABA_AR$ antagonist (gabazine 10 $\mu$M) after increasing the extracellular potassium concentration to 8 mM, but that the dynamics of the network patterns thus induced was heterogeneous and could not be compared with control cGDPs. Their amplitude and frequency significantly differed ($p < 0.05$, $n = 9$) (supplemental Fig. 2, available at www.jneurosci.org as supplemental material). In particular, large-amplitude (342 ± 7% of control, $n = 6$), low-frequency (31 ± 4% of control, $n = 6$) synchronizations appeared, associated with three-times slower calcium events (average decay was 336 ± 57% of control, $n = 4$, $p = 0.03$). In 6 of 9 experiments in high potassium conditions, large population events could be observed. These events, which invaded the entire slice including regions that did not display any synchronous activity pattern in control, are likely to correspond to the occurrence of epileptiform activity. To conclude, both cENOs and cGDPs are complex emergent network patterns that cannot be reliably mimicked by pharmacological manipulations.

The slow kinetics of cENO-associated calcium and electrophysiological events, the tonic glutamate current, as well as the immature synaptic connectivity and neuronal excitability around birth in the neocortex (Corlew et al., 2004; Moody and Bosma, 2005) suggested that the action of glutamate during cENOs could

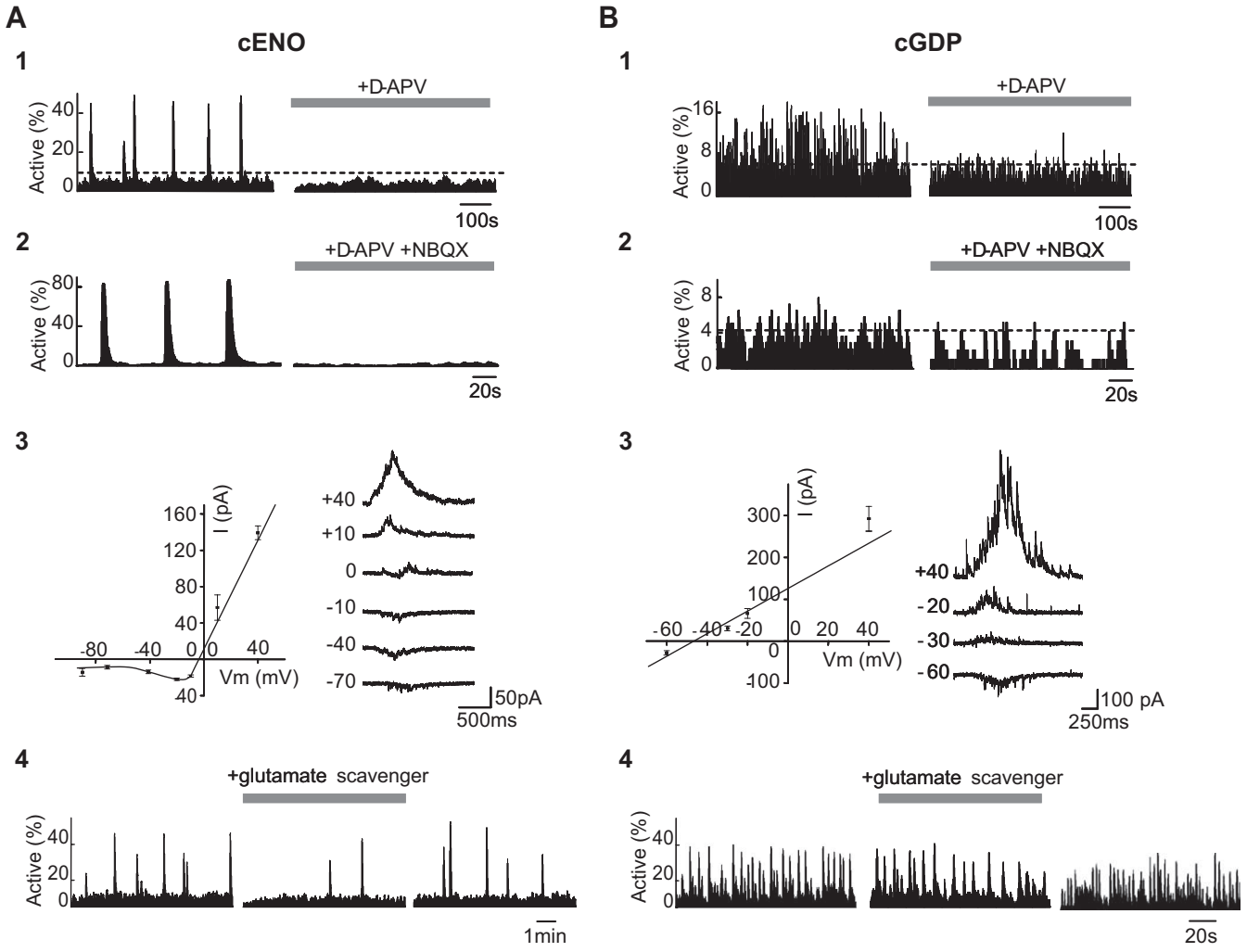


**Figure 5.** Differential role of glutamate in the generation of cortical ENOs and GDPs. ***A1***, Histograms indicating the fraction of imaged cells detected as being active for each movie frame as a function of time in a P0 somatosensory horizontal slice. The occurrence of cENOs (peaks of synchrony, left histogram) was strongly reduced when the NMDAR antagonist (D-APV, 40 $\mu$M) was added to the saline (right histogram). Dashed horizontal line indicates statistical significance threshold. ***A2***, Same type of histograms as in ***A1*** showing that the occurrence of cENOs was fully blocked in the presence of both NMDAR and AMPA/KAR antagonists (D-APV, 40 $\mu$M and NBQX, 10 $\mu$M, right histogram). ***A3***, Left, Average current–voltage relationship of cENO-associated postsynaptic currents (PSCs, 5 cENOs-PSCs averaged for each point) obtained in a representative cortical neuron. *I/V* curve displays a negative slope at negative membrane potential values and reverses around 0 mV, indicating a strong contribution of NMDARs. Error bars indicate SEM. Right, Representative traces of PSCs associated with cENOs at different holding potentials from the same recorded neuron. ***A4***, Same type of histograms as in ***A1*** in a P1 somatosensory horizontal slice, showing that perfusion with the enzymatic glutamate scavenger (GPT 5 U/ml with pyruvate 2 mM) significantly reduces the frequency of cENOs (peaks of synchrony). The effect of GPT is reversible upon wash out of the drug (right histogram). ***B***, Same as ***A*** but in P6 somatosensory horizontal slices where cGDPs could be recorded (small peaks of synchrony). ***B1***, D-APV had a significantly smaller effect on the occurrence of cGDPs compared with cENOs (see ***A1***). Dashed horizontal line indicates significance threshold; ***B2***, Blockade of ionotropic glutamatergic transmission almost completely prevented the occurrence of cGDPs. ***B3***, Same as ***A3***, but current–voltage relationship of cGDP-PSCs is linear and reverses close to −50 mV, indicating a strong contribution of $GABA_A$Rs. ***B4***, Same experiments as in ***A4*** but in a P8 slice, showing that GPT (5 U/ml) does not affect cGDPs as much as cENOs (see ***A4***).

also involve transmitter diffusion or accumulation in the extracellular space. In a first attempt to test this hypothesis, we altered the spatiotemporal glutamate profile without interfering with transmitter release or with glutamate receptors uptake mechanisms (Min et al., 1998). We used glutamic-pyruvic transaminase (GPT, alanine transaminase, EC 2.6.1.2) an enzymatic glutamate scavenger to enhance the clearance of glutamate. GPT (5 U/ml) applied together with pyruvate (2 mM) catalyzes the conversion of glutamate and pyruvate to $\alpha$-ketoglutarate. Test experiments were performed to confirm the specificity of the scavenger for glutamate (see Materials and Methods). We observed that perfusion with GPT (5 U/ml) significantly prevented the occurrence of cENOs (cENOs frequency and amplitude decreased to 19 ± 8% and 49 ± 13% of control values respectively, $n = 9$ slices, 2426 cells, $p < 0.001$) (Figs. 5, 7*B*) compared with cGDPs (frequency was 99 ± 22% of control, $p = 0.67$). If the frequency of cGDPs was not affected by the glutamate scavenger, the fraction of cells involved in them was modified since cGDPs amplitude decreased to 64 ± 7% of control values in the presence of GPT ($n = 7$ slices, 2195 cells, $p = 0.03$) (Fig. 5). Separate voltage-clamp recordings were performed to verify that GPT (5 U/ml and pyruvate) did not block evoked NMDAR-mediated synaptic currents (supplemental Fig. 3, available at www.jneurosci.org as supplemental material).

These experiments therefore argued for a critical role of glutamate and NMDAR activation in the generation of cENOs but not cGDPs. Since increases of extracellular glutamate concentration leading to transmitter diffusion are frequently associated to anoxic brain episodes (Volterra et al., 1994; Takahashi et al., 1997; Rossi et al., 2000; Auld and Robitaille, 2003) and since most

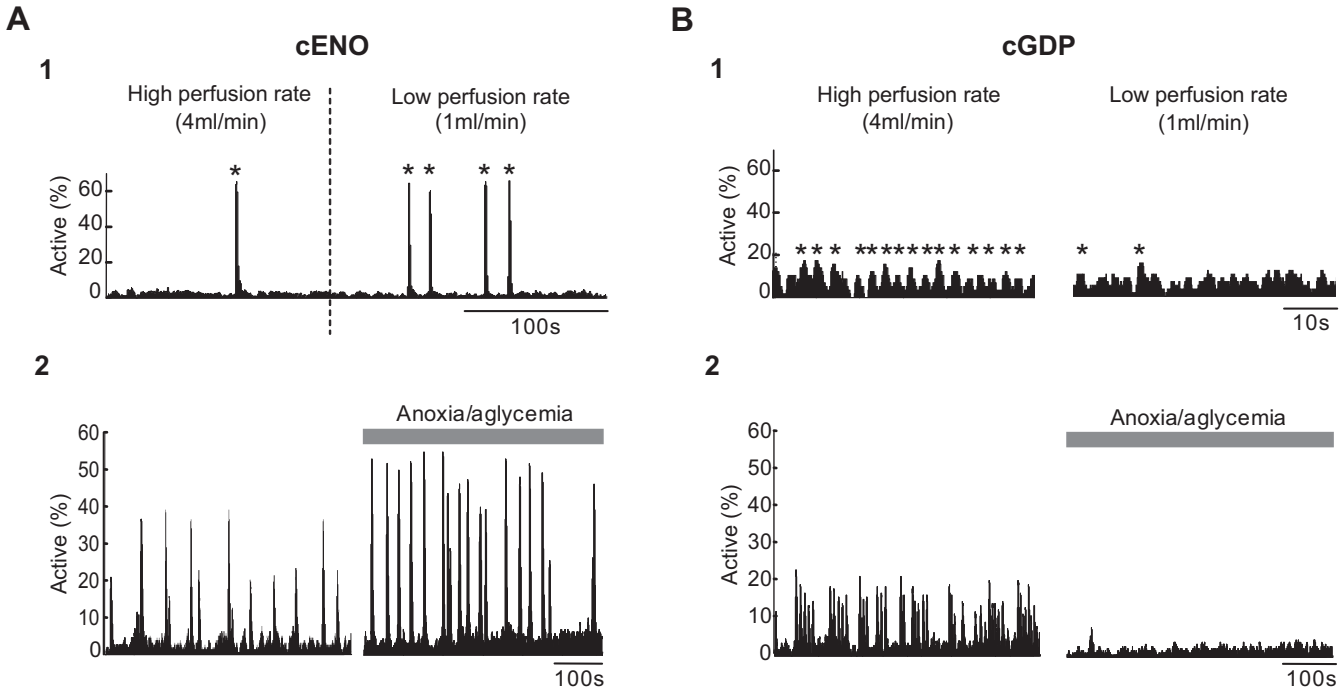


**Figure 6.** Perfusion rate and anoxic/aglycemic episodes differentially affect cENOs and cGDPs. ***A1***, Histograms indicating the fraction of imaged cells detected as being active for each movie frame as a function of time in a P2 somatosensory horizontal slice. The frequency of cENOs (peaks of synchrony indicated by *) was significantly increased when decreasing the rate of ACSF perfusion from 4 to 1 ml/min. Dashed line indicates the time when perfusion rate was modified. ***A2***, Same histograms as in ***A1*** in a P3 horizontal cortical slice. The frequency of cENOs (peaks of synchrony in the histogram) was significantly increased compared with control (left histogram) after 5 min of anoxia/aglycemia (right). ***B1***, ***B2***, Same as ***A*** but in a P7 somatosensory horizontal slice where cGDPs could be recorded (small peaks of synchrony indicated by *). In contrast to cENOs (***A***), the frequency of cGDPs was dramatically decreased in low perfusion conditions (***B1***, right) as well as after 5 min of anoxia/aglycemia (***B2***, right).

previous experiments describing cENOs were performed at relatively low perfusion rates (~1 ml/min, Corlew et al., 2004), we hypothesized that cENOs could be favored by slowing down perfusion or triggering anoxic conditions. Thus, decreasing the perfusion rate (from 4 to 1 ml/min) significantly increased the frequency of ENOs (to 359 ± 156% of control values, $n = 4$ slices, 1232 cells, $p = 0.005$) (Fig. 6). On the contrary, as reported in the hippocampus (Dzhala et al., 1999), the occurrence of cGDPs was impaired by a similar procedure (to 45 ± 26%, $n = 2$ slices, 227 cells) (Fig. 6).

We also tested the temperature dependence of both patterns and observed that their occurrence was stable between 30 and 34°C, but significantly decreased by lowering the temperature to room temperature values (~22°C, data not shown). Interestingly, when reproducing the previously described "temperature drop" protocol (Yuste et al., 1995) that consists in perfusing slices with a bolus of cold saline (~4°C), we could trigger synchronous calcium events in neuronal clusters clearly resembling "neuronal domains" (Yuste et al., 1992; Yuste et al., 1995, $n = 2$ slices, data not shown). Brief episodes (~5 min) of anoxia/aglycemia were induced by superfusion with a solution in which oxygen was substituted for nitrogen and glucose for sucrose (Dzhala et al., 1999). These experimental conditions differentially affected cENOs and cGDPs since we observed: (1) in experiments performed when cENOs dominate the neocortical network (P0–P3), a transient but significant increase in the frequency of cENOs occurring ~2 min after the beginning of anoxic conditions (to 234 ± 54% of control values, $n = 9$, $p = 0.03$) (Figs. 6, 7*A*); in addition, a significant increase of cENOs amplitude was observed just after reoxygenation (to 124 ± 9% of control values, $n = 9$, $p = 0.01$); (2) a significant reduction in the frequency and amplitude of cGDPs during anoxia and persisting up to 8 min after reoxygenation (to 25 ± 17% and 24 ± 15% of control values respectively, $n = 4$, $p = 0.03$) (Figs. 6, 7*A*). We conclude that cENOs are physiologically present in horizontal slices but favored by hypoxic conditions, most likely due to their strong dependence on glutamate levels. In contrast, experimental anoxia depresses cGDPs, which emerge later during development.

Still, cENOs and cGDPs could be the expression of the same network pattern supported by different cellular mechanisms because they are observed at separated developmental stages as described for cholinergic oscillations (Dupont et al., 2006) or retinal waves (Syed et al., 2004). To test this hypothesis, we performed experiments during the transition period (P4–P5) between ENO- and GDP-dominated networks. In a rare portion of imaged slices (2 of 17), we could simultaneously image two network patterns with significantly distinct dynamics (Fig. 7): (1) slow ENO-like calcium waves involving a large fraction of cells and occurring on average 2 times/min and (2) faster GDP-like recurrent (0.12 Hz) synchronizations between localized groups of neurons. Both patterns most likely corresponded to simultaneously imaged cENOs and cGDPs since the former was selectively blocked when the enzymatic glutamate scavenger GPT was added to the saline, whereas the latter was specifically impaired in anoxic/aglycemic conditions (Fig. 7). We conclude that cENOs and cGDPs are two distinct network patterns.

## Discussion

The main finding of the present study is that NMDAR-driven ENOs and $GABA_A$R-driven GDPs are two distinct network patterns, sequentially expressed in immature neocortical structures, characterized by different spatiotemporal dynamics both in elec-

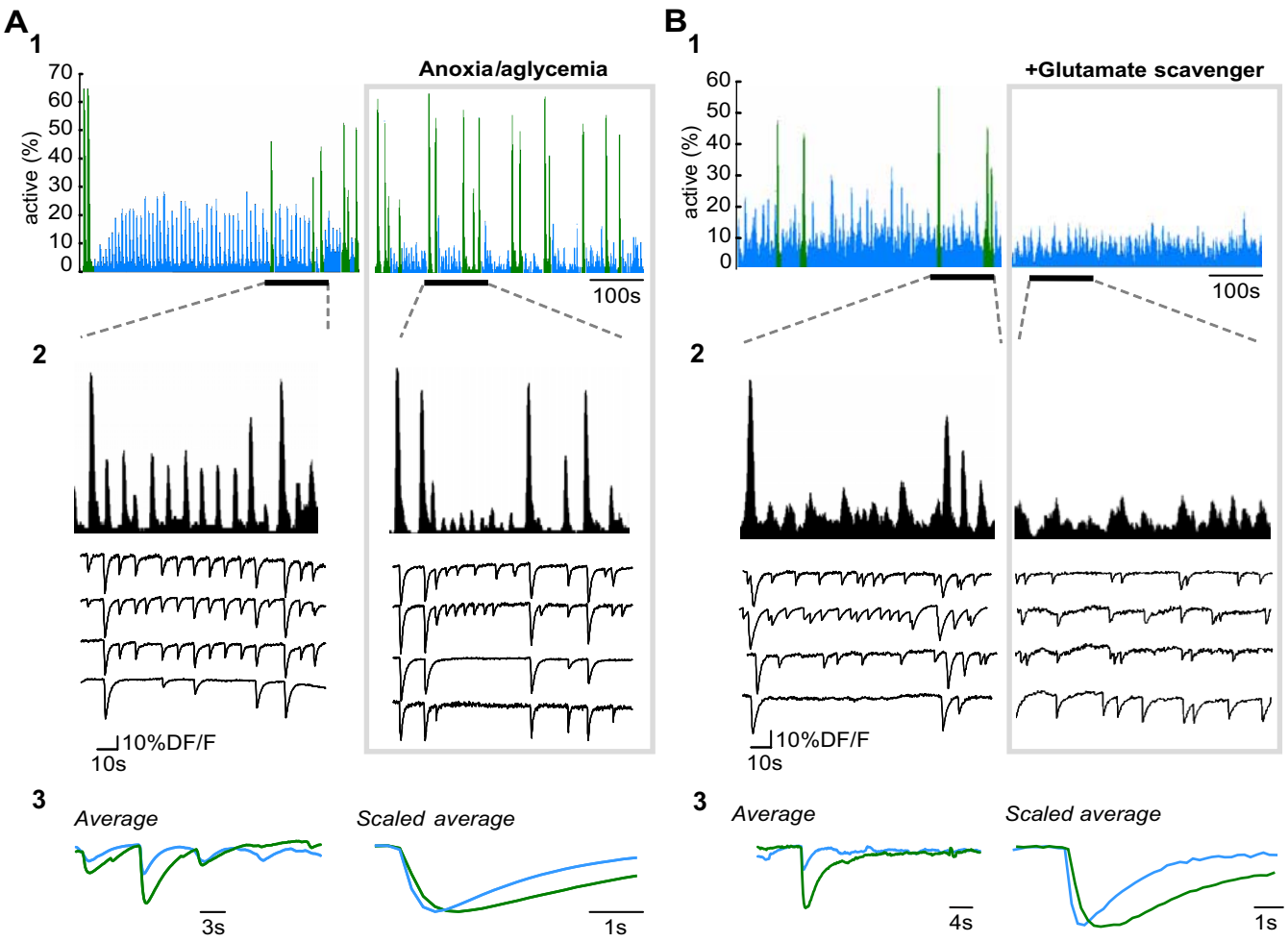


**Figure 7.** Differential modulation of cENOs and cGDPs, simultaneously recorded in a neocortical slice. ***A1***, Histograms indicating the fraction of imaged cells detected as being active for each movie frame as a function of time in a P5 somatosensory horizontal slice in control (left) and during anoxic/aglycemic conditions (right, 164 ms per frame). Two types of synchronous network events can be distinguished: cGDPs (blue) are smaller amplitude highly recurrent synchronizations associated to fast and small amplitude calcium transients and cENOs (green) are less frequent large peaks of synchrony associated to slower and larger calcium transients. Perfusion with anoxic/aglycemic ACSF increases the frequency of cENOs but reduces that of cGDPs. ***A2***, Same histograms as in ***A1*** but on an expanded time scale for the time period indicated in ***A1*** by a horizontal bar. Representative calcium fluorescence traces from four imaged cells illustrating the amplitude and kinetics difference between cENO and cGDP-associated calcium events. ***A3***, Comparison of all the digitally averaged calcium fluorescence events associated to cENOs (green) and cGDPs (blue) from the entire duration of the recording clearly indicates the amplitude difference between the two network patterns. Comparison of the scaled digital averages shows that the rise and decay time constants of cENOs-associated calcium transients are significantly slower than those associated to cGDPs (rise time: 1.0 vs 0.6 s; decay: 5.7 vs 1.6 s). ***B***, Same as ***A***, but comparing control and perfusion with the enzymatic glutamate scavenger (GPT 5 U/ml with pyruvate 2 mM) Perfusion with GPT (5 U/ml) selectively blocks the occurrence of cENOs (green) without significantly affecting cGDPs (blue).

trical and optical recordings. Most importantly, we show that cENOs are effectively modulated by extracellular glutamate levels. This unique feature imparts to the immature cerebral cortex a critical sensitivity to pathological transmitter accumulations, such as those occurring during anoxic episodes.

### Electrophysiological and single-cell correlates of calcium oscillations in the immature neocortex

In this study we have chosen to perform a compound description of population activity to gain the best resolution and assess the spatiotemporal features of any organized activity pattern, even discrete and localized. Whereas activity is poorly correlated at embryonic stages, large scale calcium waves abruptly emerge at birth in horizontal neocortical slices; these calcium events correspond to the extensively described ENOs (Garaschuk et al., 2000; Corlew et al., 2004; McCabe et al., 2006, 2007) as they present similar dynamics (i.e., calcium kinetics, amplitude, rate of occurrence), developmental profile, temperature sensitivity, and pharmacological properties. Most imaging studies describing cENOs (Garaschuk et al., 2000; Corlew et al., 2004; McCabe et al., 2006, 2007) were performed in horizontal slices and surprisingly we could indeed record them only in ~5% of imaged coronal slices. This would indicate that cENOs are better supported when some anatomical connections are spared, most likely the rostrocaudal organization within layers rather than the intralaminar circuitry (Fleidervish et al., 1998). In agreement with this, spontaneous oscillatory network activity similar to cENOs could be recorded with MEA chips in thick coronal cortical slices, but much more infrequently (Sun and Luhmann, 2007). In our study we confirmed that cENOs are associated with (1) field potential oscillations and increased multiunit activity (MUA) validating that they result from synchronous population discharges; (2) sustained membrane potential depolarization that could lead to action potential firing; and (3) a barrage of NMDAR driven EPSCs. This work therefore provides the first comprehensive description of the electrophysiological correlates underlying cENOs.

**Cortical ENOs and cGDPs are different network patterns**

One recent study aimed at separating between different oscillatory network electrical activities (Sun and Luhmann, 2007) using MEA recordings but the description was restricted to P0–P3 and a clear correlate with calcium imaging studies could not be established. Here we find that cENOs and cGDPs represent different patterns since:

First, the expression of cENOs peaks around birth (P0–P3) and they are no longer present when cGDPs dominate the network (P6–P8). There is a transition period (P4–P5) during which both patterns can be simultaneously recorded. Second, cENO-associated calcium events are five times slower than cGDPs and neuronal activity builds up within ~1 s in contrast to cGDPs that synchronize neurons within <200 ms. Also, cENOs-associated membrane potential oscillations are 10 times slower (3 s on average) than cGDP-associated events. Even at their expression peak (P0–P3), cENOs are rare events compared with cGDPs which are on average 4 times more frequent. Moreover, cENOs are large propagating waves that involve most neurons in contrast to GDPs which are often confined involving on average only one tenth of the imaged population. This difference indeed reflects different generating and propagating mechanisms (see below). In addition, cENOs are largely supported by synaptic NMDAR but not $GABA_AR$ activation, in contrast to cGDPs, and depend on extracellular glutamate concentrations as initially hypothesized (Garaschuk et al., 2000). Indeed, cENOs are blocked by a glutamate scavenger. Moreover, we show that a tonic NMDAR-mediated glutamate current most likely contributes to the resting membrane potential and excitability of some neurons preferentially at the stage where cENOs are expressed. However, it should be noted that real resting membrane potential conditions are difficult to assess at early stages when neurons are small due to errors in measurement (Tyzio et al., 2003). Interestingly, NMDAR activation has been critically implicated in several cortical oscillations at early developmental stages, including most pharmacologically induced patterns (Dupont et al., 2006; Demarque et al., 2004). A variation in the subunit composition of NMDARs in intracortical synapses (Kumar and Huguenard, 2003; Nevian and Sakmann, 2004; Pérez-Otaño et al., 2006), a weaker sensitivity to magnesium block near resting potential (Ben-Ari et al., 1988; Fleidervish et al., 1998; Binshtok et al., 2006; Cattani et al., 2007) or high glutamate affinity are features that should support their activation by ambient glutamate. Finally, cENOs and cGDPs are differentially affected by anoxic conditions since slowing down the perfusion rate and/or producing mild anoxic conditions blocks cGDPs and increases the frequency of cENOs. Blockade of hippocampal GDPs in similar conditions results from a depression of synaptic activity by endogenous adenosine released during anoxia acting via presynaptic receptors (Dzhala et al., 1999).

ENOs are likely to be a pattern specific to developing neocortical structures. A particular sensitivity of neocortical neurons to glutamate transport function (Furuta et al., 1997; Kidd and Isaac, 2000; Demarque et al., 2004) and a specific expression of functionally distinct NMDARs might explain this restricted expression of ENOs in the neocortex. In contrast to cENOs, SPAs can be recorded both in the hippocampus (Crépel et al., 2007) and neocortex; SPAs therefore seem a general pattern of network maturation. As in the hippocampus, cortical SPAs peaked at birth, were boosted by application of the maternal hormone oxytocin and started declining when cGDPs could be observed. SPAs and cENOs shared similar developmental profiles and could occur synchronously but the exact interaction between these two patterns needs to be further investigated; cSPAs could be involved in the generation of cENOs by providing, for example, few cells with a depolarized membrane potential suitable for NMDAR activation.

Interestingly, cENOs and cGDPs coexist during a short period. If future studies are required to understand the cellular basis for the handover of synchrony between cENOs and cGDPs, a maturation of glutamate transporters function (Demarque et al., 2004), a developmental switch in NMDAR properties in neocortical neurons (Crair and Malenka, 1995; Pérez-Otaño et al., 2006), a decline of the SPA pattern and a postnatal development of GABAergic circuits (Chattopadhyaya et al., 2004; Hensch and Stryker, 2004; Minlebaev et al., 2007) are likely to be critical determinants for this transition.

***In vivo* correlates and possible function of early cortical activity patterns**

Studies in neonatal rodents *in vivo* have characterized an early pattern of synchronized cortical electrical activity (Khazipov et al., 2004; Hanganu et al., 2006; Khazipov and Luhmann, 2006; Minlebaev et al., 2007), the "spindle-bursts" that are most likely homologous to human premature delta brushes recorded in EEG (Milh et al., 2007b). Due to their comparable dynamics (i.e., rate of occurrence, duration), similarly confined spatial distribution and developmental profile (Khazipov et al., 2004; Hanganu et al., 2006; Khazipov and Luhmann, 2006; Minlebaev et al., 2007), "spindle bursts" could be the *in vivo* expression of slice cGDPs. Besides, the disappearance of both spindle bursts and delta brushes tightly parallels the maturation of functional GABAergic inhibition supporting a crucial implication of this neurotransmitter in their generation (Dzhala et al., 2005; Vanhatalo et al., 2005). However, only a small fraction of the *in vivo* spindle bursts are intrinsically generated in the cortex independently from the periphery (Khazipov et al., 2004; Hanganu et al., 2006; Khazipov and Luhmann, 2006; Minlebaev et al., 2007). Therefore, future studies combining *in vivo* cellular calcium imaging and electrical recordings are required to clarify the link between cGDPs and spindle bursts.

Cortical calcium waves sharing similarities with slice cENOs have been described *in vivo* in unanesthetized rats by recordings of the integrated calcium signal from populations of cells (Adelsberger et al., 2005). The major common point between these *in vivo* calcium waves and slice cENOs was that they propagated to the entire cortical mantle in contrast to "spindle bursts." But it is worth noting that *in vivo* calcium waves occurred more frequently and at later developmental stages than *in vitro* ENOs (Garaschuk et al., 2000; Adelsberger et al., 2005). This study therefore strongly suggests that the *in vivo* counterpart of cENOs is likely to be an endogenous brain rhythm expressed during sleep-like resting states and disappearing during the animal movement (Adelsberger et al., 2005). Unfortunately, the *in vivo* pattern of electrical activity as well as the human EEG correlate of cENOs remains to be determined. The normal EEG of premature infants displays a wide variety of discontinuous activity patterns as a function of age (Lamblin et al., 1999; Vanhatalo et al., 2002; Tolonen et al., 2007; Vecchierini et al., 2007). Furthermore, full band EEG recordings indicate the initial abundance of very slow activity patterns that could translate into cENOs (Vanhatalo et al., 2002; Tolonen et al., 2007; Vecchierini et al., 2007). Finding the *in vivo* electrical pattern corresponding to cENOs will require recordings in unanesthetized animals around birth.

Probably the most unique property of cENOs is their being enhanced by anoxic conditions. It is the first time, to our knowl-

edge, that a developmental network pattern was shown not to be altered but rather reinforced by pathological conditions. This property most likely derives from the strong sensitivity of cENOs to extracellular glutamate levels. Glutamate uptake by astrocytes was shown to be disrupted by hypoxia (Dallas et al., 2007). The astrocytic network might indeed be implicated in the control of cENOs even in normoxic conditions (Aguado et al., 2002). Interestingly, hypoxic-ischemic encephalopathy in human neonates is very often associated to discontinuous EEG patterns including "suppression bursts," which dynamics and suggested cellular mechanisms can be intriguingly similar to cENOs (Biagioni et al., 1999; Ohtahara and Yamatogi, 2003; Demarque et al., 2004; Milh et al., 2007a). Future studies should determine whether indeed ischemic episodes within a critical window period of fetal development will lead to the replay or the ongoing of primitive cortical oscillations.

## References


Adelsberger H, Garaschuk O, Konnerth A (2005) Cortical calcium waves in resting newborn mice. Nat Neurosci 8:988–990.

Aguado F, Espinosa-Parrilla JF, Carmona MA, Soriano E (2002) Neuronal activity regulates correlated network properties of spontaneous calcium transients in astrocytes in situ. J Neurosci 22:9430–9444.

Auld DS, Robitaille R (2003) Glial cells and neurotransmission: an inclusive view of synaptic function. Neuron 40:389–400.

Ben-Ari Y, Cherubini E, Krnjevic K (1988) Changes in voltage dependence of NMDA currents during development. Neurosci Lett 94:88–92.

Ben-Ari Y, Cherubini E, Corradetti R, Gaiarsa JL (1989) Giant synaptic potentials in immature rat CA3 hippocampal neurones. J Physiol 416:303–325.

Ben-Ari Y, Gaiarsa JL, Tyzio R, Khazipov R (2007) GABA: a pioneer transmitter that excites immature neurons and generates primitive oscillations. Physiol Rev 87:1215–1284.

Biagioni E, Bartalena L, Boldrini A, Pieri R, Cioni G (1999) Constantly discontinuous EEG patterns in full-term neonates with hypoxic-ischaemic encephalopathy. Clin Neurophysiol 110:1510–1515.

Binshtok AM, Fleidervish IA, Sprengel R, Gutnick MJ (2006) NMDA receptors in layer 4 spiny stellate cells of the mouse barrel cortex contain the NR2C subunit. J Neurosci 26:708–715.

Cang J, Rentería RC, Kaneko M, Liu X, Copenhagen DR, Stryker MP (2005) Development of precise maps in visual cortex requires patterned spontaneous activity in the retina. Neuron 48:797–809.

Cattani AA, Bonfardin VD, Represa A, Ben-Ari Y, Aniksztejn L (2007) Generation of slow network oscillations in the developing rat hippocampus after blockade of glutamate uptake. J Neurophysiol 98:2324–2336.

Chattopadhyaya B, Di Cristo G, Higashiyama H, Knott GW, Kuhlman SJ, Welker E, Huang ZJ (2004) Experience and activity-dependent maturation of perisomatic GABAergic innervation in primary visual cortex during a postnatal critical period. J Neurosci 24:9598–9611.

Corlew R, Bosma MM, Moody WJ (2004) Spontaneous, synchronous electrical activity in neonatal mouse cortical neurones. J Physiol 560:377–390.

Crair MC, Malenka RC (1995) A critical period for long-term potentiation at thalamocortical synapses. Nature 375:325–328.

Crépel V, Aronov D, Jorquera I, Represa A, Ben-Ari Y, Cossart R (2007) A parturition-associated nonsynaptic coherent activity pattern in the developing hippocampus. Neuron 54:105–120.

Dallas M, Boycott HE, Atkinson L, Miller A, Boyle JP, Pearson HA, Peers C (2007) Hypoxia suppresses glutamate transport in astrocytes. J Neurosci 27:3946–3955.

Dammerman RS, Flint AC, Noctor S, Kriegstein AR (2000) An excitatory GABAergic plexus in developing neocortical layer 1. J Neurophysiol 84:428–434.

Demarque M, Villeneuve N, Manent JB, Becq H, Represa A, Ben-Ari Y, Aniksztejn L (2004) Glutamate transporters prevent the generation of seizures in the developing rat neocortex. J Neurosci 24:3289–3294.

Dupont E, Hanganu IL, Kilb W, Hirsch S, Luhmann HJ (2006) Rapid developmental switch in the mechanisms driving early cortical columnar networks. Nature 439:79–83.

Dzhala V, Desfreres L, Melyan Z, Ben-Ari Y, Khazipov R (1999) Epileptogenic action of caffeine during anoxia in the neonatal rat hippocampus. Ann Neurol 46:95–102.

Dzhala VI, Talos DM, Sdrulla DA, Brumback AC, Mathews GC, Benke TA, Delpire E, Jensen FE, Staley KJ (2005) NKCC1 transporter facilitates seizures in the developing brain. Nat Med 11:1205–1213.

Fleidervish IA, Binshtok AM, Gutnick MJ (1998) Functionally distinct NMDA receptors mediate horizontal connectivity within layer 4 of mouse barrel cortex. Neuron 21:1055–1065.

Furuta A, Rothstein JD, Martin LJ (1997) Glutamate transporter protein subtypes are expressed differentially during rat CNS development. J Neurosci 17:8363–8375.

Garaschuk O, Hanse E, Konnerth A (1998) Developmental profile and synaptic origin of early network oscillations in the CA1 region of rat neonatal hippocampus. J Physiol 507:219–236.

Garaschuk O, Linn J, Eilers J, Konnerth A (2000) Large-scale oscillatory calcium waves in the immature cortex. Nat Neurosci 3:452–459.

Hanganu IL, Ben-Ari Y, Khazipov R (2006) Retinal waves trigger spindle bursts in the neonatal rat visual cortex. J Neurosci 26:6728–6736.

Hensch TK, Stryker MP (2004) Columnar architecture sculpted by GABA circuits in developing cat visual cortex. Science 303:1678–1681.

Kandler K, Gillespie DC (2005) Developmental refinement of inhibitory sound-localization circuits. Trends Neurosci 28:290–296.

Kandler K, Katz LC (1998) Coordination of neuronal activity in developing visual cortex by gap junction-mediated biochemical communication. J Neurosci 18:1419–1427.

Katz LC, Shatz CJ (1996) Synaptic activity and the construction of cortical circuits. Science 274:1133–1138.

Khazipov R, Luhmann HJ (2006) Early patterns of electrical activity in the developing cerebral cortex of humans and rodents. Trends Neurosci 29:414–418.

Khazipov R, Sirota A, Leinekugel X, Holmes GL, Ben-Ari Y, Buzsáki G (2004) Early motor activity drives spindle bursts in the developing somatosensory cortex. Nature 432:758–761.

Kidd FL, Isaac JT (2000) Glutamate transport blockade has a differential effect on AMPA and NMDA receptor-mediated synaptic transmission in the developing barrel cortex. Neuropharmacology 39:725–732.

Kumar SS, Huguenard JR (2003) Pathway-specific differences in subunit composition of synaptic NMDA receptors on pyramidal neurons in neocortex. J Neurosci 23:10074–10083.

Lamblin MD, André M, Challamel MJ, Curzi-Dascalova L, d'Allest AM, De Giovanni E, Moussalli-Salefranque F, Navelet Y, Plouin P, Radvanyi-Bouvet MF, Samson-Dollfus D, Vecchierini-Blineau MF (1999) [Electroencephalography of the premature and term newborn. Maturational aspects and glossary]. Neurophysiol Clin 29:123–219.

Marandi N, Konnerth A, Garaschuk O (2002) Two-photon chloride imaging in neurons of brain slices. Pflugers Arch 445:357–365.

McCabe AK, Chisholm SL, Picken-Bahrey HL, Moody WJ (2006) The self-regulating nature of spontaneous synchronized activity in developing mouse cortical neurones. J Physiol 577:155–167.

McCabe AK, Easton CR, Lischalk JW, Moody WJ (2007) Roles of glutamate and GABA receptors in setting the developmental timing of spontaneous synchronized activity in the developing mouse cortex. Dev Neurobiol 67:1574–1588.

Milh M, Becq H, Villeneuve N, Ben-Ari Y, Aniksztejn L (2007a) Inhibition of glutamate transporters results in a "suppression-burst" pattern and partial seizures in the newborn rat. Epilepsia 48:169–174.

Milh M, Kaminska A, Huon C, Lapillonne A, Ben-Ari Y, Khazipov R (2007b) Rapid cortical oscillations and early motor activity in premature human neonate. Cereb Cortex 17:1582–1594.

Min MY, Rusakov DA, Kullmann DM (1998) Activation of AMPA, kainate, and metabotropic receptors at hippocampal mossy fiber synapses: role of glutamate diffusion. Neuron 21:561–570.

Minlebaev M, Ben-Ari Y, Khazipov R (2007) Network mechanisms of spindle-burst oscillations in the neonatal rat barrel cortex in vivo. J Neurophysiol 97:692–700.

Moody WJ, Bosma MM (2005) Ion channel development, spontaneous activity, and activity-dependent development in nerve and muscle cells. Physiol Rev 85:883–941.

Nevian T, Sakmann B (2004) Single spine $Ca^{2+}$ signals evoked by coincident EPSPs and backpropagating action potentials in spiny stellate cells of layer 4 in the juvenile rat somatosensory barrel cortex. J Neurosci 24:1689–1699.

Nicol X, Voyatzis S, Muzerelle A, Narboux-Nême N, Südhof TC, Miles R, Gaspar P (2007) cAMP oscillations and retinal activity are permissive for ephrin signaling during the establishment of the retinotopic map. Nat Neurosci 10:340–347.

Ohtahara S, Yamatogi Y (2003) Epileptic encephalopathies in early infancy with suppression-burst. J Clin Neurophysiol 20:398–407.

Owens DF, Kriegstein AR (1998) Patterns of intracellular calcium fluctuation in precursor cells of the neocortical ventricular zone. J Neurosci 18:5374–5388.

Owens DF, Boyce LH, Davis MB, Kriegstein AR (1996) Excitatory GABA responses in embryonic and neonatal cortical slices demonstrated by gramicidin perforated-patch recordings and calcium imaging. J Neurosci 16:6414–6423.

Pérez-Otaño I, Luján R, Tavalin SJ, Plomann M, Modregger J, Liu XB, Jones EG, Heinemann SF, Lo DC, Ehlers MD (2006) Endocytosis and synaptic removal of NR3A-containing NMDA receptors by PACSIN1/syndapin1. Nat Neurosci 9:611–621.

Rossi DJ, Oshima T, Attwell D (2000) Glutamate release in severe brain ischaemia is mainly by reversed uptake. Nature 403:316–321.

Sipilä ST, Huttu K, Soltesz I, Voipio J, Kaila K (2005) Depolarizing GABA acts on intrinsically bursting pyramidal neurons to drive giant depolarizing potentials in the immature hippocampus. J Neurosci 25:5280–5289.

Sun JJ, Luhmann HJ (2007) Spatio-temporal dynamics of oscillatory network activity in the neonatal mouse cerebral cortex. Eur J Neurosci 26:1995–2004.

Syed MM, Lee S, Zheng J, Zhou ZJ (2004) Stage-dependent dynamics and modulation of spontaneous waves in the developing rabbit retina. J Physiol 560:533–549.

Takahashi M, Billups B, Rossi D, Sarantis M, Hamann M, Attwell D (1997) The role of glutamate transporters in glutamate homeostasis in the brain. J Exp Biol 200:401–409.

Tolonen M, Palva JM, Andersson S, Vanhatalo S (2007) Development of the spontaneous activity transients and ongoing cortical activity in human preterm babies. Neuroscience 145:997–1006.

Tyzio R, Ivanov A, Bernard C, Holmes GL, Ben-Ari Y, Khazipov R (2003) Membrane potential of CA3 hippocampal pyramidal cells during postnatal development. J Neurophysiol 90:2964–2972.

Tyzio R, Cossart R, Khalilov I, Minlebaev M, Hübner CA, Represa A, Ben-Ari Y, Khazipov R (2006) Maternal oxytocin triggers a transient inhibitory switch in GABA signaling in the fetal brain during delivery. Science 314:1788–1792.

Tyzio R, Holmes GL, Ben-Ari Y, Khazipov R (2007) Timing of the developmental switch in GABA(A) mediated signaling from excitation to inhibition in CA3 rat hippocampus using gramicidin perforated patch and extracellular recordings. Epilepsia 48 [Suppl 5]:96–105.

Vanhatalo S, Tallgren P, Andersson S, Sainio K, Voipio J, Kaila K (2002) DC-EEG discloses prominent, very slow activity patterns during sleep in preterm infants. Clin Neurophysiol 113:1822–1825.

Vanhatalo S, Palva JM, Andersson S, Rivera C, Voipio J, Kaila K (2005) Slow endogenous activity transients and developmental expression of K+-Cl- cotransporter 2 in the immature human cortex. Eur J Neurosci 22:2799–2804.

Vecchierini MF, André M, d'Allest AM (2007) Normal EEG of premature infants born between 24 and 30 weeks gestational age: terminology, definitions and maturation aspects. Neurophysiol Clin 37:311–323.

Volterra A, Trotti D, Tromba C, Floridi S, Racagni G (1994) Glutamate uptake inhibition by oxygen free radicals in rat cortical astrocytes. J Neurosci 14:2924–2932.

Yamada J, Okabe A, Toyoda H, Kilb W, Luhmann HJ, Fukuda A (2004) Cl- uptake promoting depolarizing GABA actions in immature rat neocortical neurones is mediated by NKCC1. J Physiol 557:829–841.

Yuste R, Katz LC (1991) Control of postsynaptic Ca2+ influx in developing neocortex by excitatory and inhibitory neurotransmitters. Neuron 6:333–344.

Yuste R, Peinado A, Katz LC (1992) Neuronal domains in developing neocortex. Science 257:665–669.

Yuste R, Nelson DA, Rubin WW, Katz LC (1995) Neuronal domains in developing neocortex: mechanisms of coactivation. Neuron 14:7–17.